




## Gyre turbulence: Anomalous dissipation in a two-dimensional ocean model

Lennard Miller <sup>1,2,\*</sup>, Bruno Deremble <sup>2,†</sup> and Antoine Venaille <sup>1,‡</sup>

<sup>1</sup>ENS de Lyon, CNRS, Laboratoire de Physique (UMR CNRS 5672), F-69342 Lyon, France

<sup>2</sup>Université Grenoble Alpes, CNRS, INRAE, IRD, Grenoble-INP, Institut des Géosciences de l'Environnement, 38400 Grenoble, France



(Received 3 October 2023; revised 25 November 2023; accepted 4 March 2024; published 3 May 2024)

The exploration of a two-dimensional wind-driven ocean model with no-slip boundaries reveals the existence of a turbulent asymptotic regime where energy dissipation becomes independent of fluid viscosity. This asymptotic flow represents an out-of-equilibrium state, characterized by a vigorous two-dimensional vortex gas superimposed onto a western-intensified gyre. The properties of the vortex gas are elucidated through scaling analysis for detached Prandtl boundary layers, providing a rationalization for the observed anomalous dissipation. The asymptotic regime demonstrates that boundary instabilities alone can be strong enough to evacuate wind-injected energy from the large-scale oceanic circulation.

DOI: [10.1103/PhysRevFluids.9.L051801](https://doi.org/10.1103/PhysRevFluids.9.L051801)

*Introduction.* In three-dimensional turbulence, the transfer of energy from large to small scales results in an energy dissipation rate that remains independent of viscosity, regardless of its smallness [1,2]. This dissipative anomaly is a robust empirical observation sometimes referred to as the zeroth law of turbulence [3]. Conversely, two-dimensional flows are subject to an inverse energy cascade [4], which results in the self-organization of the flow at the domain scale [5]. To ensure efficient dissipation in two-dimensional flows, an additional mechanism is required to generate small-scale structures where dissipation can operate, thus disrupting the inverse cascade. The strong shear near lateral boundaries could serve as a means to create such dissipative structures [6]. Numerical studies of the bounded Navier-Stokes equations have examined the relationship between dissipation and viscosity during a dipole-wall collision [7–9]. The possibility for dissipation to remain finite in the inviscid limit has been raised [10,11], yet remains a topic of debate [12,13].

The existence of a dissipative anomaly in two-dimensional flows with boundaries would bear significant practical implications, for example, in contributing to a deeper understanding of the energy cycle in the ocean [14–17]. In fact, classical linear models for the emergence of western-intensified currents [18,19], such as the Gulf Stream or the Kuroshio, do provide a remarkable example of a dissipative anomaly. Here, we show that this dissipative anomaly persists in a nonlinear regime, and unveil a gyre turbulence regime with a western-intensified mean flow and finite-energy dissipation rate.

*Flow model.* The simplest model describing western intensification of oceanic currents is the rigid-lid barotropic quasigeostrophic model on a closed domain tangent to the Earth [18]:

$$\partial_t \omega + J(\psi, \omega) + \beta^* \partial_x \psi = \nu^* \Delta \omega - \partial_y \tau, \quad (1)$$

$$\omega = \Delta \psi, \quad \tau = -\cos(\pi y). \quad (2)$$

\*lennard.miller@univ-grenoble-alpes.fr

†bruno.deremble@univ-grenoble-alpes.fr

‡antoine.venaille@ens-lyon.fr

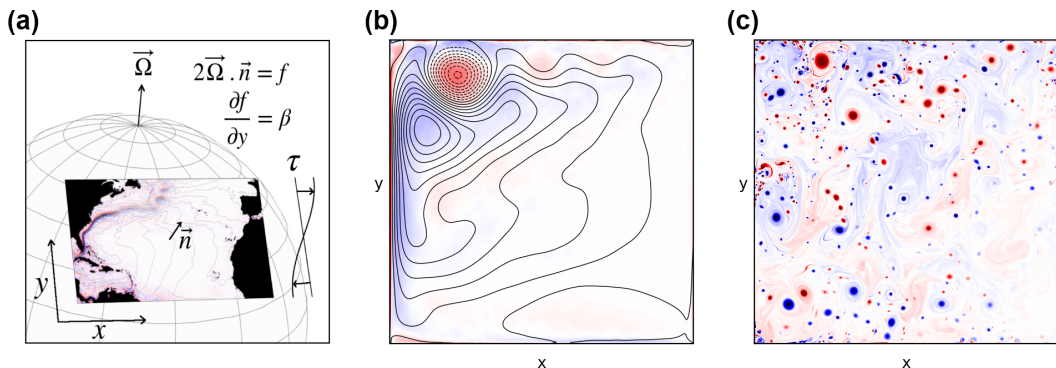


FIG. 1. (a) The  $\beta$ -plane model with an inlet for the streamlines of the time-average sea surface velocity field in the North Atlantic. Colors show the corresponding relative vorticity field. (b) Temporal average of the streamlines in the gyre turbulence regime ( $\nu^* = 2.5 \times 10^{-5}$ ), superimposed on the corresponding relative vorticity field (colors). (c) Snapshot of relative vorticity in the gyre turbulence regime ( $\nu^* = 2 \times 10^{-6}$ ). Blue: anticyclonic vortices; red: cyclonic vortices (see Supplemental Material [33] movie S2 for an animation).

The term  $J(\psi, \omega) = (u\partial_x + v\partial_y)\omega$  is the advection of vorticity  $\omega$  by the stream function  $\psi$ , with  $u = -\partial_y\psi$  the zonal ( $x$ -direction) and  $v = \partial_x\psi$  the meridional ( $y$ -direction) velocity components. We solve this two-dimensional model on a square domain with no-slip boundary conditions. Forcing comes from the wind stress curl  $-\partial_y\tau$ . Time and length have been rescaled such that both the length of the domain  $L$  and the maximum value of the wind stress  $\tau_0$  are 1. The shape of the forcing corresponds to a single gyre, and is somewhat relevant to the North Atlantic case, with net injection of negative vorticity, as observed in the subtropical gyre [Fig. 1(a)]. The only difference to the incompressible two-dimensional Navier-Stokes equations is the term  $\beta^*\partial_x\psi$ . This term comes from the curl of the Coriolis force, assuming linear variations of the Coriolis parameter in the meridional direction  $y$ . This framework is called the  $\beta$ -plane approximation, and it captures the effects of differential rotation induced by a rotating planet [18].

Earlier studies of the single-gyre model with free-slip boundary conditions exhibited an inertial runaway in the inviscid limit: a solution with unrealistically large velocities, and lacking an intensified western boundary current [20–26]. One way to prevent this inertial runaway is to use no-slip conditions [27–29]. It was also noticed that no-slip boundary conditions in two-dimensional turbulence can drastically alter flow organization [30–32]. In the context of a wind-driven shallow water model, Ref. [29] observed that no-slip conditions induced the intermittent formation of intense vortices through boundary layer detachment. We show below that this mechanism enables the large-scale flow to remain in an oceanic gyre regime when considering the inviscid limit of Eqs. (1) and (2) (see Supplemental Material [33] movie S1 for a direct comparison of the free-slip against the no-slip regimes).

*Linear dynamics.* Linear theories for wind-driven gyres compute steady states of Eqs. (1) and (2), by neglecting the advection term [18,19]. In the domain bulk, the vorticity equation simplifies into the Sverdrup balance, a cornerstone of midlatitude ocean dynamics,  $\beta^*v = -\partial_y\tau$ , meaning that an injection of negative vorticity is balanced by a southward transport of the fluid. To ensure mass conservation, this interior circulation must be complemented by boundary layers. The majority of this recirculation occurs within the western boundary layer, thereby breaking the East-West symmetry established by the Sverdrup balance. In the viscous solution found by Munk [Fig. 2(a), top left inset] the boundary layer thickness scales as  $\delta_M = (\nu^*/\beta^*)^{1/3}$  [34], which implies that total dissipation is dominated by contributions from the boundary layer while energy injection comes from the domain bulk. The confinement of energy dissipation in a western boundary layer holds when viscosity is replaced by other dissipation mechanisms, such as a linear drag [18]. In this scenario, large-scale gyre patterns and therefore energy injection do not depend on details of those

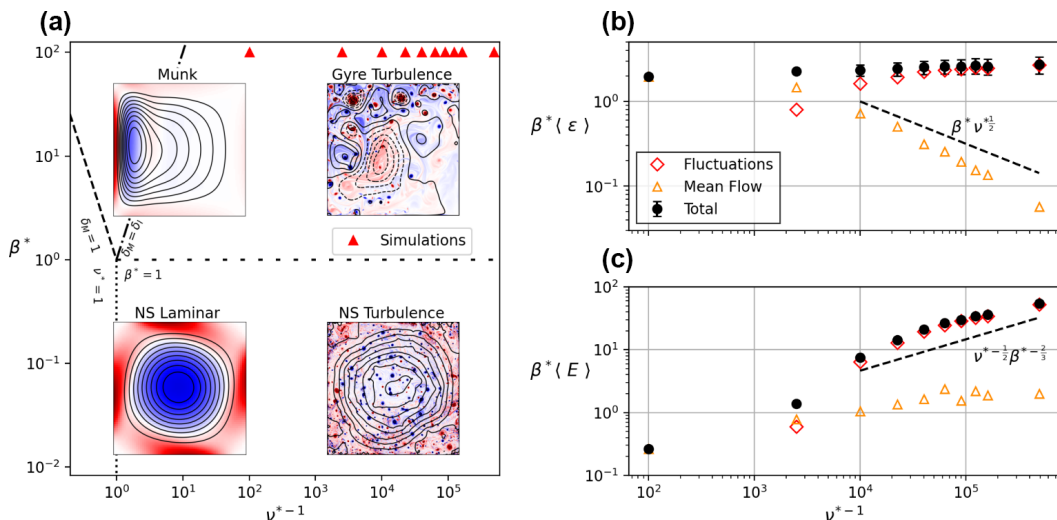


FIG. 2. (a) Parameter space (no-slip boundary conditions). Insets show typical instantaneous vorticity fields (color) and stream functions (lines). (b) Energy dissipation rate, rescaled by the energy injection through a Sverdrup interior. (c) Energy rescaled by the energy of the inertial western boundary layer. Error bars show the standard deviation.

linear boundary layers. This is a strong incentive to look for a turbulent dissipative anomaly in this system, adding back nonlinearities into the problem.

*Parameter regimes.* The linear Munk solution is a limiting case in the  $(\nu^*, \beta^*)$  parameter space, corresponding to  $\beta^* \gg 1$  and a restricted range of  $\nu^*$  to be discussed below. The parameter space can be dissected into four regions [Fig. 2(a)]: In the limit of weak  $\beta^*$ , the effects of differential rotation are negligible with respect to other terms and the flow response is equivalent to that of the two-dimensional Navier-Stokes (NS) equations, with a transition from laminar to turbulent flow when  $\nu^*$  decreases [31]. The same transition from laminar to turbulent flow occurs when differential rotation is important ( $\beta^* \gg 1$ ). When  $\nu^* = 10^{-2}$ , we observe that the flow consists of a domain interior in which a Sverdrup balance holds with a stationary western boundary layer, similar to the linear Munk solution.

When viscosity is decreased, the boundary layer becomes increasingly inertial and its thickness will be governed by  $\delta_I = \beta^{*-1}$  [18,35]. The transition between the laminar Munk regime and this inertial regime occurs around  $\delta_M = \delta_I$ , i.e.,  $\nu^* = 1/\beta^{*2}$ . When viscosity is decreased further below this threshold, the boundary layer becomes unstable, and those instabilities feed the domain with filaments and vortices. As friction is further reduced the system eventually enters into the gyre turbulence regime: While the time mean flow remains close to a Sverdrup interior with western-intensified boundary layers [Fig. 1(b)], the instantaneous vorticity field is dominated by a vigorous heterogeneous vortex gas which is densest in the northwestern corner of the domain [Fig. 1(c); for an animation, see Supplemental Material [33] movie S2]. The gyre structure is not observed on instantaneous stream-function fields, which is instead dominated by contributions arising from Rossby basin modes [36] (not shown here), and to a lesser extent by contributions from vortices.

*Energy budget.* The central result of this Letter is depicted in Fig. 2(b) showing that the dissipative anomaly of the linear Munk regime persists in the nonlinear gyre turbulence regime. Dissipation  $\epsilon$  appears in the energy budget as

$$\frac{\partial E}{\partial t} = \mathcal{P} - \epsilon, \quad \mathcal{P} = \int \tau u dA, \quad \epsilon = 2\nu^* Z, \quad (3)$$

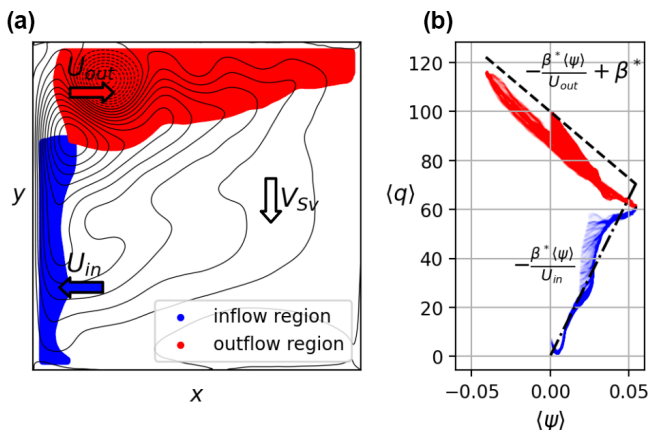


FIG. 3. (a) Contour plot of the mean stream function  $\langle \psi \rangle$  at  $\nu^* = 2.5 \times 10^{-5}$ , with colored areas identified as inertial boundary layers. (b)  $q - \psi$  relations in the inertial boundary layers.

where  $E = \int (u^2 + v^2) dA/2$  is the total energy and  $Z = \int \omega^2 dA/2$  the total enstrophy. We define time average and fluctuations as

$$\langle \psi \rangle = \lim_{T \rightarrow \infty} \frac{1}{T} \int_s^{s+T} \psi dt, \quad \psi' = \psi - \langle \psi \rangle, \quad (4)$$

where the integration is started from a moment  $s$  in time after which the system is observed to be in statistical equilibrium, for which  $\langle \mathcal{P} \rangle = \langle \varepsilon \rangle$ .

In gyre turbulence, the average dissipation  $\langle \varepsilon \rangle$  is observed to be insensitive to a decrease in  $\nu^*$  [Fig. 2(b)]. Our rescaling by  $\beta^{*-1}$  shows that the dissipation rate remains close to that predicted by energy injection through an interior flow governed by a Sverdrup balance. However, the dissipation mechanism changes drastically as fluctuations become increasingly important at smaller values of  $\nu^*$ , while the mean flow contributes only a negligible fraction to the total dissipation. The importance of the fluctuations can also be seen in the total energy of the flow [Fig. 2(c)]. The rescaling by  $\beta^{*-1}$  reveals that the total energy of the mean flow remains close to the energy in a western inertial boundary layer, while the magnitude of the fluctuations increases when  $\nu^*$  decreases. To rationalize these observations, we describe below the mean flow structure (related to energy injection), and the production of filaments and vortices (related to energy dissipation).

*Mean flow structure.* In the gyre turbulence regime, the time-averaged production term  $\langle \mathcal{P} \rangle$  must be independent of  $\nu^*$ , as it balances the time-averaged dissipation  $\langle \varepsilon \rangle$ . This constraint, together with the observation in Fig. 2(b) that the energy of the mean flow reaches a plateau, suggests that the bulk stream function  $\langle \psi \rangle$  displayed in Fig. 1(b) only has a weak dependence on  $\nu^*$  in the gyre turbulence regime. While the order of magnitude of the mean flow agrees with Sverdrup balance in the domain interior [Fig. 3(a)], the gyre pattern is different than the prediction from linear theory, likely due to nonlinear rectification mechanisms in the presence of Rossby waves [32,37]. We observe only weak changes in this pattern when lowering viscosity in the gyre turbulence regime (see Supplemental Material [33] Fig. 2).

The gyre pattern is connected to inertial boundary layers with a well-defined functional relation between stream function and potential vorticity  $\langle q \rangle = \langle \omega \rangle + \beta y$ , such that  $J(\langle q \rangle, \langle \psi \rangle) = 0$ . We identified two regions where such relations hold (Fig. 3), which we will call the inflow (blue) and the outflow (red) layer. The inflow layer is consistent with classical theory predicting  $\langle q \rangle = -(\beta^*/U_{in})\langle \psi \rangle$ , which leads to a western boundary layer thickness  $\delta_I = 1/\beta^*$ , where  $U_{in} < 0$  is the westward inflow scaling as  $1/\beta^*$  [18,35]. The northward velocity in the inertial boundary layer is  $U_I \sim 1$ , so that mass transport in this layer compensates the southward Sverdrup bulk transport.

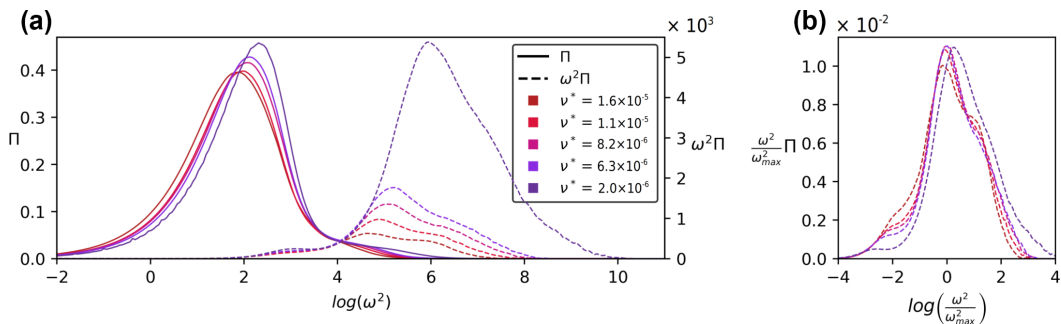


FIG. 4. (a) Probability distribution functions  $\Pi$  of  $\log(\omega^2)$  for different values of  $\nu^*$ . Also shown are the values responsible for dissipation,  $\omega^2\Pi$ . (b) Values responsible for dissipation after rescaling by  $\omega_{\max} = 1/\sqrt{\nu^*}$ . The area under the curves is equal to the total dissipation  $\langle \varepsilon \rangle$ .

A no-slip boundary condition is guaranteed by a Prandtl sublayer with thickness  $\delta_P \sim \sqrt{\nu^*}$ . The vorticity within this Prandtl layer is

$$\omega_{\max} = \frac{U_I}{\delta_P} \sim \frac{1}{\sqrt{\nu^*}}. \quad (5)$$

Assuming that dissipation of the mean flow is governed by these viscous sublayers yields

$$\nu^* \int \langle \omega \rangle^2 dA \sim \nu^* \omega_{\max}^2 \delta_P \sim \nu^{*\frac{1}{2}}, \quad (6)$$

which compares well against the observed dissipation due to the mean flow [see Fig. 2(b)].

The outflow layer close to the northern boundary corresponds to a meandering jet with velocity  $U_{\text{out}}$  and a strong cyclonic recirculation. In this area, we observe a negative correlation between  $\langle q \rangle$  and  $\langle \psi \rangle$ . A stationary Rossby wave meanders and a stationary vortex on a  $\beta$  plane with mean flow  $U_{\text{out}}$  both select the size  $\delta_{\text{out}} \sim \sqrt{U_{\text{out}}/\beta^*}$ . We assume that this length sets the vortex and jet width, and that jet transport is set by the transport of the western boundary layer, which yields

$$\delta_{\text{out}} \sim \beta^{*-2/3} \quad \text{and} \quad U_{\text{out}} \sim \beta^{*-1/3}. \quad (7)$$

An adaptation of classical Charney theory to this inertial region leads to  $\langle q \rangle = -\beta^*/U_{\text{out}}\langle \psi \rangle + \beta^*$ , which fits well with numerical results [see Fig. 3(b) and Supplemental Material [33] for further information on boundary layers].

*Statistics of dissipation.* While the production term  $\langle \mathcal{P} \rangle$  depends crucially on the mean flow, we showed that, in the turbulent regime, the dissipation term is dominated by contributions from fluctuations of vorticity [Fig. 2(b)]. Since dissipation is proportional to enstrophy, we show the probability distribution function of  $\omega^2$  in Fig. 4(a) (we checked that the distribution of  $\omega^2$  is close to the distribution of local dissipation  $|\nabla \cdot \mathbf{u}|^2$ ). The core of the distribution  $\Pi[\log(\omega^2)]$  is close to a Gaussian distribution, similar to recent observations from more comprehensive ocean models [17].

The peak of  $\Pi[\log(\omega^2)]$  changes little upon varying the viscosity, revealing that most of the values of vorticity in the bulk are only weakly dependent on  $\nu^*$ . A much stronger dependence on  $\nu^*$  is observed in the tails of the distributions, where we notice important deviations from lognormality. In fact, the average dissipation is dominated by contributions from the tails, which can be seen by plotting the quantity  $\omega^2\Pi$ . We show these tails in Fig. 4(b) after rescaling the vorticity by  $\omega_{\max}$  defined in (5), collapsing the tails onto a single curve centered around unity. This confirms that the primary mechanism for vorticity injection is the detachment of the Prandtl layer. This scaling for the vorticity can now be used to estimate the energy dissipation rate.

*Scaling analysis of the vortex gas.* The cyclonic recirculation we observe in the mean flow is a signature of the presence of intense cyclonic vortices in this region [see Fig. 1(c)]. These large vortices result from the coalescence of smaller vortices in the interior. If the vortices grow too large,

their drift velocity overcomes the advective velocity from the detached jet, and the vortex collides with the wall, detaching the sublayer over a length  $\delta_{\text{out}}$  (see Supplemental Material [33] movie S2).

Building upon this observation, the theory for the mean flow, and the observed statistics of the dissipation, it is possible to propose a scaling theory that predicts the  $\nu^*$  dependency of the energy of the vortex gas. For this, we suppose that the energy is determined by  $N$  characteristic vortices of size  $\lambda$ . If we assume that the vortices are created by the roll-up of the detached sublayer of the western boundary along a length  $\delta_{\text{out}}$ , then the characteristic vortex radius scales as  $\lambda \sim \sqrt{\delta_{\text{out}}\delta\rho}$ . Furthermore, in the inviscid limit we observe a balance between the dissipation of these vortices and the injection of energy through the mean Sverdrup flow. The balance between energy dissipation through the characteristic vortices and injection through a Sverdrup interior takes the form

$$\nu^* N \lambda^2 \omega_{\text{max}}^2 \sim \beta^{*-1}. \quad (8)$$

This determines the area fraction of the vortices as  $N\lambda^2 \sim \beta^{*-1}$ , which we verify (see Supplemental Material [33] Fig. 2). The total energy of the vortex gas is then given by

$$E \sim N \lambda^2 (\omega_{\text{max}} \lambda)^2 \sim \nu^{*-1/2} \beta^{*-5/3}, \quad (9)$$

with additional logarithmic corrections [38]. Although the ideas behind this scaling do not incorporate the fragmentation or coalescence and the resulting inhomogeneity of the vortex gas, a reasonable agreement between simulations and this scaling theory is observed [Fig. 2(c)].

*Discussion.* Our study challenges the consensus that a weakly dissipated two-dimensional ocean model would lead to energy accumulation due to the absence of a forward energy cascade [16,18]. Instead, no-slip boundaries offer a compelling route to dissipation, sustaining low-energy western-intensified gyres with a vigorous vortex gas. This gyre turbulence regime is a genuine out-of-equilibrium state defying description using equilibrium statistical mechanics [2,5], or quasilinear approaches [39,40].

Originally discovered in freely decaying two-dimensional (2D) flows [41], the vortex gas regime emerges in baroclinically unstable stratified quasigeostrophic flows or any two-dimensional flow with forcing amplifying vorticity extrema [38,42–45]. Gyre turbulence, lacking bulk instabilities, generates intense vortex cores solely at the boundary layers. The interplay of a western boundary and the  $\beta$  effect also seems to prevent crystallization previously observed on a polar cap [46], although this feature may yet occur at lower viscosity not attained in the presented simulations. A quantitative description of the large-scale gyre pattern will require an examination of potential vorticity mixing induced by the vortex gas, as in Refs. [38,47,48].

In the broader context of the real ocean, turbulent western boundaries have long been recognized as significant energy sinks [15], with the potential for a linear forward cascade mediated by planetary vorticity gradients [49] and intense vortex generation through boundary layer detachment [29]. Our study reveals that incompressible two-dimensional  $\beta$ -plane turbulence serves as a minimal model sustaining wind gyres coexisting with mesoscale vortices that contain the majority of the flow energy. However, the two-dimensional model falls short in capturing the fate of these vortices, as evidenced by their energy increase with  $\nu^{*-1/2}$ . Three-dimensional and ageostrophic effects [16,50], interactions with bottom topography [51–53], and air-sea interactions [54] are expected to play vital roles in dissipating these fine-scale structures. We conjecture that a large part of the energy flux toward these fine scales will continue to be governed by larger scales, a hypothesis currently under examination using more comprehensive ocean models.

*Acknowledgments.* This project has received financial support from the CNRS through the 80 Prime program, and was performed using HPC resources from GENCI-TGCC (Grant No. 2022-A0130112020). We warmly thank G. Roulet for insightful inputs on this topic.

---

[1] U. Frisch, *Turbulence: The Legacy of A. N. Kolmogorov* (Cambridge University Press, Cambridge, U.K., 1995).



- [2] G. L. Eyink and K. R. Sreenivasan, Onsager and the theory of hydrodynamic turbulence, *Rev. Mod. Phys.* **78**, 87 (2006).
- [3] B. Dubrulle, Beyond Kolmogorov cascades, *J. Fluid Mech.* **867**, P1 (2019).
- [4] G. Boffetta and R. E. Ecke, Two-dimensional turbulence, *Annu. Rev. Fluid Mech.* **44**, 427 (2012).
- [5] F. Bouchet and A. Venaille, Statistical mechanics of two-dimensional and geophysical flows, *Phys. Rep.* **515**, 227 (2012).
- [6] B. Deremble, W. K. Dewar, and E. P. Chassignet, Vorticity dynamics near sharp topographic features, *J. Mar. Res.* **74**, 249 (2016).
- [7] H. J. H. Clercx and G. J. F. van Heijst, Dissipation of kinetic energy in two-dimensional bounded flows, *Phys. Rev. E* **65**, 066305 (2002).
- [8] W. Kramer, H. J. H. Clercx, and G. J. F. van Heijst, Vorticity dynamics of a dipole colliding with a no-slip wall, *Phys. Fluids* **19**, 126603 (2007).
- [9] G. H. Keetels, W. Kramer, H. J. H. Clercx, and G. J. F. van Heijst, On the Reynolds number scaling of vorticity production at no-slip walls during vortex-wall collisions, *Theor. Comput. Fluid Dyn.* **25**, 293 (2011).
- [10] R. Nguyen van yen, M. Farge, and K. Schneider, Energy dissipating structures produced by walls in two-dimensional flows at vanishing viscosity, *Phys. Rev. Lett.* **106**, 184502 (2011).
- [11] M. Waidmann, R. Klein, M. Farge, and K. Schneider, Energy dissipation caused by boundary layer instability at vanishing viscosity, *J. Fluid Mech.* **849**, 676 (2018).
- [12] D. Sutherland, C. Macaskill, and D. G. Dritschel, The effect of slip length on vortex rebound from a rigid boundary, *Phys. Fluids* **25**, 093104 (2013).
- [13] H. J. H. Clercx and G. J. F. van Heijst, Dissipation of coherent structures in confined two-dimensional turbulence, *Phys. Fluids* **29**, 111103 (2017).
- [14] R. Ferrari and C. Wunsch, Ocean circulation kinetic energy: Reservoirs, sources, and sinks, *Annu. Rev. Fluid Mech.* **41**, 253 (2009).
- [15] X. Zhai, H. L. Johnson, and D. P. Marshall, Significant sink of ocean-eddy energy near western boundaries, *Nat. Geosci.* **3**, 608 (2010).
- [16] A. Pouquet and R. Marino, Geophysical turbulence and the duality of the energy flow across scales, *Phys. Rev. Lett.* **111**, 234501 (2013).
- [17] B. Pearson and B. Fox-Kemper, Log-normal turbulence dissipation in global ocean models, *Phys. Rev. Lett.* **120**, 094501 (2018).
- [18] G. K. Vallis, *Atmospheric and Oceanic Fluid Dynamics* (Cambridge University Press, Cambridge, U.K., 2017).
- [19] A.-L. Dalibard and L. Saint-Raymond, Mathematical study of degenerate boundary layers: A large scale ocean circulation problem, *Mem. Am. Math. Soc.* **253** (2018).
- [20] V. Kamenkovich, V. Sheremet, A. Pastushkov, and S. Belotserkovsky, Analysis of the barotropic model of the subtropical gyre in the ocean for finite Reynolds numbers. Part I, *J. Mar. Res.* **53**, 959 (1995).
- [21] V. Sheremet, V. Kamenkovich, and A. Pastushkov, Analysis of the barotropic model of the subtropical gyre in the ocean for finite Reynolds numbers. Part II, *J. Mar. Res.* **53**, 995 (1995).
- [22] G. Ierley and V. Sheremet, Multiple solutions and advection-dominated flows in the wind-driven circulation. Part I: Slip, *J. Mar. Res.* **53**, 703 (1995).
- [23] V. Sheremet, G. Ierley, and V. Kamenkovich, Eigenanalysis of the two-dimensional wind-driven ocean circulation problem, *J. Mar. Res.* **55**, 57 (1997).
- [24] F. Dupont and D. N. Straub, Effect of a wavy wall on the single gyre Munk problem, *Tellus A: Dyn. Meteorol. Oceanogr.* **56**, 387 (2004).
- [25] P. S. Berloff, J. C. McWilliams, and A. Bracco, Material transport in oceanic gyres. Part I: Phenomenology, *J. Phys. Oceanogr.* **32**, 764 (2002).
- [26] B. Fox-Kemper and J. Pedlosky, Wind-driven barotropic gyre I: Circulation control by eddy vorticity fluxes to an enhanced removal region, *J. Mar. Res.* **62**, 169 (2004).
- [27] P. Cessi, R. V. Condie, and W. Young, Dissipative dynamics of western boundary currents, *J. Mar. Res.* **48**, 677 (1990).

- [28] H. Nakano, H. Tsujino, and R. Furue, The Kuroshio current system as a jet and twin relative recirculation gyres embedded in the Sverdrup circulation, *Dynam. Atmos. Oceans* **45**, 135 (2008).
- [29] C. Q. C. Akuetevi and A. Wirth, Dynamics of turbulent western-boundary currents at low latitude in a shallow-water model, *Ocean Sci.* **11**, 471 (2015).
- [30] H. J. H. Clercx, S. R. Maassen, and G. J. F. Van Heijst, Decaying two-dimensional turbulence in square containers with no-slip or stress-free boundaries, *Phys. Fluids* **11**, 611 (1999).
- [31] H. J. H. Clercx, G. J. F. Van Heijst, D. Molenaar, and M. G. Wells, No-slip walls as vorticity sources in two-dimensional bounded turbulence, *Dynam. Atmos. Oceans* **40**, 3 (2005).
- [32] W. Kramer, M. G. van Buren, H. J. H. Clercx, and G. J. F. van Heijst,  $\beta$ -plane turbulence in a basin with no-slip boundaries, *Phys. Fluids* **18**, 026603 (2006).
- [33] See Supplemental Material at <http://link.aps.org/supplemental/10.1103/PhysRevFluids.9.L051801> for details on numerical methods, boundary layer analysis, and movies.
- [34] W. H. Munk, On the wind-driven ocean circulation, *J. Atmos. Sci.* **7**, 80 (1950).
- [35] J. G. Charney, The Gulf stream as an inertial boundary layer, *Proc. Natl. Acad. Sci. USA* **41**, 731 (1955).
- [36] J. Pedlosky, *Geophysical Fluid Dynamics* (Springer, Berlin, 2013).
- [37] B. Fox-Kemper, Wind-driven barotropic gyre II: Effects of eddies and low interior viscosity, *J. Mar. Res.* **62**, 195 (2004).
- [38] B. Gallet and R. Ferrari, The vortex gas scaling regime of baroclinic turbulence, *Proc. Natl. Acad. Sci. USA* **117**, 4491 (2020).
- [39] B. Gallet and W. R. Young, A two-dimensional vortex condensate at high Reynolds number, *J. Fluid Mech.* **715**, 359 (2013).
- [40] A. Frishman and C. Herbert, Turbulence statistics in a two-dimensional vortex condensate, *Phys. Rev. Lett.* **120**, 204505 (2018).
- [41] J. C. McWilliams, The emergence of isolated coherent vortices in turbulent flow, *J. Fluid Mech.* **146**, 21 (1984).
- [42] B. K. Arbic and G. R. Flierl, Baroclinically unstable geostrophic turbulence in the limits of strong and weak bottom Ekman friction: Application to midocean eddies, *J. Phys. Oceanogr.* **34**, 2257 (2004).
- [43] A. F. Thompson and W. R. Young, Scaling baroclinic eddy fluxes: Vortices and energy balance, *J. Phys. Oceanogr.* **36**, 720 (2006).
- [44] A. Venaille, G. K. Vallis, and K. S. Smith, Baroclinic turbulence in the ocean: Analysis with primitive equation and quasigeostrophic simulations, *J. Phys. Oceanogr.* **41**, 1605 (2011).
- [45] A. van Kan, B. Favier, K. Julien, and E. Knobloch, Spontaneous suppression of inverse energy cascade in instability-driven 2-D turbulence, *J. Fluid Mech.* **952**, R4 (2022).
- [46] L. Siegelman, W. R. Young, and A. P. Ingersoll, Polar vortex crystals: Emergence and structure, *Proc. Natl. Acad. Sci. USA* **119**, e2120486119 (2022).
- [47] B. Gallet and R. Ferrari, A quantitative scaling theory for meridional heat transport in planetary atmospheres and oceans, *AGU Adv.* **2**, e2020AV000362 (2021).
- [48] L. Siegelman and W. R. Young, Two-dimensional turbulence above topography: Vortices and potential vorticity homogenization, *Proc. Natl. Acad. Sci. USA* **120**, e2308018120 (2023).
- [49] B. T. Nadiga and D. N. Straub, Alternating zonal jets and energy fluxes in barotropic wind-driven gyres, *Ocean Model.* **33**, 257 (2010).
- [50] D. Balwada, J.-H. Xie, R. Marino, and F. Feraco, Direct observational evidence of an oceanic dual kinetic energy cascade and its seasonality, *Sci. Adv.* **8**, eabq2566 (2022).
- [51] W. K. Dewar and A. M. Hogg, Topographic inviscid dissipation of balanced flow, *Ocean Model.* **32**, 1 (2010).
- [52] M. Nikurashin, G. K. Vallis, and A. Adcroft, Routes to energy dissipation for geostrophic flows in the southern ocean, *Nat. Geosci.* **6**, 48 (2013).
- [53] L.-F. Zhang and J.-H. Xie, Spectral condensation in quasi-geostrophic turbulence above small-scale topography, [arXiv:2311.16612](https://arxiv.org/abs/2311.16612).
- [54] L. Renault, P. Marchesiello, S. Masson, and J. C. McWilliams, Remarkable control of western boundary currents by eddy killing, a mechanical air-sea coupling process, *Geophys. Res. Lett.* **46**, 2743 (2019).